metals

MDPI

Article

Aluminum Scrap to Hydrogen: Complex Effects of Oxidation Medium, Ball Milling Parameters, and Copper Additive Dispersity

Olesya A. Buryakovskaya [1,*], Musi Zh. Suleimanov [1], Mikhail S. Vlaskin [1,2,3,*], Vinod Kumar [2,3] and Grayr N. Ambaryan [1]

[1] Laboratory of Energy Accumulating Materials, Joint Institute for High Temperatures of the Russian Academy of Sciences, Moscow 125412, Russia
[2] Department of Lifesciences, Graphic Era (Deemed to Be University), Dehradun 248002, India
[3] Department of Environmental Monitoring and Forecasting, Peoples' Friendship University of Russia (RUDN University), Moscow 117198, Russia
* Correspondence: osminojishe@yandex.ru (O.A.B.); vlaskin@inbox.ru (M.S.V.)

Abstract: An effective combination of oxidation medium, ball milling parameters, and copper additive disperstiy ensuring fast aluminum scrap reaction with high hydrogen yield, was suggested. Different milling parameters (5, 10, and 15 mm steel balls; 1 and 2 h; unidirectional and bidirectional rotation modes) were tested for Al-10 wt.% Cu (50–70 μm) composition. The samples milled with 5 (2 h) and 10 mm (1 and 2 h) balls contained undesirable intermetallic phases Al_2Cu and Cu_9Al_4, while those activated with 15 mm balls (1 h) provided the second-finest powder and best preservation of the original Cu and Al phases. Among the tested (at 60 °C) 2 M solutions NaCl, LiCl, KCl, $MgCl_2$, $ZnCl_2$, $BaCl_2$, $CaCl_2$, $NiCl_2$, $CoCl_2$, $FeCl_2$, and $AlCl_3$, the first six appeared to be almost useless (below 4% hydrogen yield), the following four provided better results, and the ultimate 91.5% corresponded to $AlCl_3$. Samples with Cu dispersity of 50–100 nm, 1–19, 50–70, and 150–250 μm, and with no additive, were milled under the optimal parameters and tested in $AlCl_3$. Their total yields were similar (~90–94%), while reaction rates differed. The highest rate was obtained for the sample modified with 50–70 μm powder.

Keywords: aluminum scrap; copper powders; composite materials; ball milling; phase transformations; intermetallides; aqueous salt solutions; hydrogen generation

check for updates

Citation: Buryakovskaya, O.A.; Suleimanov, M.Z.; Vlaskin, M.S.; Kumar, V.; Ambaryan, G.N. Aluminum Scrap to Hydrogen: Complex Effects of Oxidation Medium, Ball Milling Parameters, and Copper Additive Dispersity. *Metals* **2023**, *13*, 185. https://doi.org/10.3390/met13020185

Academic Editor: Elena Gordo

Received: 26 December 2022
Revised: 10 January 2023
Accepted: 14 January 2023
Published: 17 January 2023

Copyright: © 2023 by the authors. Licensee MDPI, Basel, Switzerland. This article is an open access article distributed under the terms and conditions of the Creative Commons Attribution (CC BY) license (https://creativecommons.org/licenses/by/4.0/).

1. Introduction

Rising global challenges associated with CO_2 emissions, energy security, and sustainable development prompt scientific, political, and business communities to intensify their efforts to elaborate transformation strategies in the energy sector [1,2]. Transition to net-zero greenhouse gas emissions, circular economy, renewable energy sources, and effective heat and power systems represents an acute modern problem [3–6]. Cleaner technologies for transport and buildings have already become reality [7–9]. And yet, the major drawback of renewable energy (wind, solar, wave, tidal) is its inconsistency. Therefore, in recent years, a number of solutions for its accumulation and storage, as well as for the optimization, control, and management of its consumption have appeared [6,10,11]. One of the promising approach to solving energy accumulation, storage, and transition problems is implementation of hydrogen—sustainable and environmentally friendly fuel [12]. Currently, the major starting materials for its production are hydrocarbons (undergoing steam reforming, pyrolysis, or gasification); their promising alternatives include water (split by electrolysis) and biomass (subject to fermentation) [13–16]. Electrical water splitting, largely relying on electrocatalysts (heterointerface materials with a hierarchical morphology, carbon-based amorphous transition metal complexes, etc.), is the perfect method for large-scale hydrogen production [17,18].

On the one hand, hydrogen represents almost perfect 'fuel of the future', which can be utilized in fuel cells, gas turbines, or internal combustion engines. On the other hand, however, its use is associated with dangers arising from its low ignition energy, relatively high flame velocity, wide flammability range, and rapid diffusion [19,20]. The most popular of the existing hydrogen storage technologies are physical storage (compressed or liquid gas), and chemical storage (gas bonded to metal hydrides). Their main drawbacks are associated respectively with high pressures (up to 700–1000 bar), low temperatures (down to 20 K), and low hydrogen densities, poor reversibility, slow kinetics, and high dehydrogenation temperatures [21].

In order to avoid the mentioned obstacles, a required amount of hydrogen can be obtained in situ from the oxidation of some metals (mainly, magnesium and aluminum) with water or aqueous solution. Under normal conditions, aluminum (excepting nanoparticles) cannot react with water due to the presence of a slowly hydrated protective oxide layer on the metal's surface [22]. For micron-sized Al powders and distilled water, the reaction with hydrogen generation became observable at temperatures of 68–70 °C, but proceeded slowly [23,24]. Therefore, to induce the reaction, a number of approaches to remove the passive film have been suggested. One of such approaches constitutes in carrying out the process at temperatures above 100 °C that ensures a considerable increase on water diffusivity [25–34]. Another approach is to destroy the protective film by aluminum ball milling with various additives. The other ball milling effects are significant reduction in the aluminum particle sizes, and creation of crystal lattice imperfections, favoring pitting corrosion. Metal can be ball milled as it is, or with hard and brittle additives, such as salts (e.g., NaCl, KCl, $NiCl_2$, $CoCl_2$) [35–39], oxides and hydroxides ($Bi(OH)_3$, AlOOH, $Al(OH)_3$, Al_2O_3, TiO_2, Co_3O_4, Cr_2O_3, MoO_3, Bi_2O_3, CuO, Cu_2O) [40–46]. An important ball milling effect for Al modified with metals (e.g., Bi, Zn, In, Ni, Sn, Cu) is the formation of 'microgalvanic cells' enhancing galvanic corrosion of less noble aluminum in conductive media [47–51]. The same activation mechanism was employed for the alloy samples manufactured by aluminum melting with various metals (Fe, Sn, Cu, Bi, Sn, Li) [52–58]. Addition of Ga and Ga-based alloys (together with In, Sn, Mg, Zn, Cu) results in liquid metal embrittlement of aluminum, which undergoes cracking along the grain boundaries and readily interacts with water over its newly created surfaces [59–64]. And one more of the widely used ways to aluminum activation is dissolution of its passive layer by the transformation of aluminum oxides and hydroxides into highly soluble compounds. Thus, the reaction between alkali solutions, NaOH or KOH, and aluminum lead to the formation of aluminates, $NaAl(OH)_4$ or $KaI(OH)_4$ [65–69]. And hydrochloric acid as well as metal chlorides supply Cl^- ions which interaction with the oxide film produces oxy- and hydroxychlorides [70–74]. Utilization of waste aluminum is another modern matter of interest, as aluminum foils, wires, dross, cans, machining products, construction parts, and debris represent a cheaper starting material for hydrogen production [75–81].

In the present study, a method for the conversion of aluminum machining waste in form of chips and shavings into hydrogen will be suggested. To study the effect of solution composition on the reaction rate, 2 M aqueous solutions NaCl, LiCl, KCl, $MgCl_2$, $CaCl_2$, $ZnCl_2$, $BaCl_2$, $NiCl_2$, $CoCl_2$, $FeCl_2$, and $AlCl_3$ will be tested at a temperature of 60 °C (below the temperature of 68 °C, when aluminum-water reaction becomes detectable). Pitting corrosion of Al in the presence of Cl^- ions is affected by the material composition, presence and distribution of micro-defects (vacancies, voids, etc.) as well as macro-defects (inclusions, second phase particles, their size and shape) [82]. From the commonly used metals, Cu, Sn, Al, Ni, Fe, Zn, and Pb, corrosion potentials of Cu and Al measured in chloride solutions were the highest and the lowest [83]. To enhance aluminum corrosion in chlorine solution, its modification with Cu will be performed. In some studies, it was shown that under specific conditions, ball milling of Al with Cu leads to the formation of intermetallic phases Al_2Cu (stable) and Cu_9Al_4 (metastable, removable by annealing) [84–89] and, in case of prolonged ball milling, additional phases of solid solutions Cu(Al) or Al(Cu) [90–92]. According to the data collected from the studies on Al-Cu ball milling, prolonged ball milling and high

rotation speeds leads to the formation of the said intermetallic compounds. Their formation can be beneficial for the improvement of Al-Cu alloys mechanical properties. However, the corrosion potentials of the intermetallic phases fall between those for Al and Cu [93]. Although the new phase is 'cathodic' with respect to Al, the difference between their potentials is obviously smaller than that for Al and Cu. Also the formation of such phases consumes some amount of Al, thus decreasing the theoretical hydrogen yield. Moreover, ball milling duration and milling ball size exert big influence on the structure transformation of aluminum particles. Thus, it was demonstrated that prolonged ball milling (over 4–7 h) of aluminum powder leads to a decrease in its hydrogen generation performance, and that a smaller number of big balls provide much better powder particle size reduction as compared to a big number of small balls [44,94–96]. Therefore, another aim of the present study is investigation of the effect of ball milling parameters (duration and milling balls' sizes) on the phase composition of samples manufactured of 90 wt.% Al scrap and 10 wt.% Cu powder. The effect of additive particle sizes on hydrogen production from hydroreactive metals is not obvious as well. Thus, in study [97], for Mg-Ni composite it was assumed that a larger cathode (Ni) surface area resulting from shorter ball milling time was one of the key reasons for faster hydrogen production. In contrast, in study [98], Bi nanoparticles were reported to demonstrate better results than micron-sized ones. Therefore, for the selected solution and ball milling parameters, the influence of copper powder particle size on the hydrogen evolution performance will be studied as well.

2. Materials and Methods

The base starting material for the manufacture of hydroreactive samples was scrap of D16 grade aluminum alloy (National Standard GOST 4784–97) which elemental composition was generally similar to that of 2024 aluminum alloy [99,100]. Activator (10 wt.%) was represented by copper powders with various particle sizes: 50–100 nm nanopowder (98%, Technical Specification No. 1791-003-36280340-2008, 'MP-Line Group' Ltd., Moscow, Russia), 1–19 μm ultradisperse powder (99.999%, Technical Specification No. 1793-001-50316079-2004, 'MetallEnergoHolding', group of companies, Ltd., Irkutsk, Russia), 50–70 μm PMS-1 grade powder (99.5%, National Standard GOST 4960-2009, 'Rushim.Ru' Ltd., Moscow, Russia), and 150–250 μm PMS-N grade coarse powder (99.999%, National Standard GOST 4960-2009, 'Uralelektromed' JSC, Verkhnyaya Pyshma, Russia). 2 M aqueous salt solutions were prepared of distilled water and the following reagents: chemically pure NaCl (National Standard GOST 4233-77, 'LabTech' Ltd., Moscow, Russia), chemically pure KCl (National Standard GOST 4234-77, 'LabTech' Ltd., Moscow, Russia), pure anhydrous LiCl (Technical Specification No. 2-476-11, 'Component-Reaktiv' Ltd., Moscow, Russia), pure anhydrous $CaCl_2$ (Technical Specification No. 2-239-10, 'Component-Reaktiv' Ltd., Moscow, Russia), chemically pure $AlCl_3 \cdot 6H_2O$ (Technical Specification No. 2-191-10, 'Component-Reaktiv' Ltd., Moscow, Russia), pure $ZnCl_2$ (Technical Specification No. 1-533-12, 'Component-Reaktiv' Ltd., Moscow, Russia), analytical grade $BaCl_2 \cdot 2H_2O$ (National Standard GOST 4108-72, 'Reahim' Ltd., Moscow, Russia), $MgCl_2 \cdot 6H_2O$ (CAS 7791-18-6, 'Rushim.Ru' Ltd., Moscow, Russia), $FeCl_2 \cdot 4H_2O$ (Technical Specification No. 6-02-609-86, 'Rushim.Ru' Ltd., Moscow, Russia), $CoCl_2 \cdot 6H_2O$ (National Standard GOST 4525-77, 'Rushim.Ru' Ltd., Moscow, Russia), and pure $NiCl_2 \cdot 6H_2O$ (National Standard GOST 4038-79, 'Rushim.Ru' Ltd., Moscow, Russia).

Ball milling was performed using a centrifugal ball mill (S 100; 'Retsch' GmbH, Haan, Germany) and 125 mL milling pot which was filled in a glove box (G-BOX-F-290; 'FUMATECH' Ltd., Novosibirsk, Russia) under pure argon (99.993%, National State Standard GOST 10157-79, 'NII KM' Ltd., Moscow, Russia). To assess the effect of milling ball size, sets of stainless steel balls of 5, 10, and 15 mm in diameter were used. The ball to powder ratio of 24:1 was the same for all experiments; the ball sets included 191 small (5 mm) balls, or 24 medium size (10 mm) balls, or 7 big (15 mm) balls. To evaluate the milling duration influence, 1 and 2 h time intervals were tested. The rotation speed of 580 rpm was the same for all experiments. Two rotation modes—bidirectional, with pauses (30 s cycles,

1 s pauses), and more intensive unidirectional, without pauses—were tested in order to establish their possible influence on the formation of the said intermetallic phases and dispersity of the resulting composites.

The preparation for experiments on hydrogen evolution included pouring 1000 mL of 2 M aqueous salt solution into a reactor (1000 mL, JSC 'Lenz Laborglas', Wertheim, Germany) and heating it up to 60 °C with a heater (CC-308B; JSC 'ONE Peter Huber Kältemaschinenbau', Offenburg, Germany) under stirring (300 rpm) with a magnetic mixer (C-MAG HS 7; JSC 'IKA-Werke', Staufen, Germany). Then a 0.5 g sample was loaded into the reactor. Generated hydrogen passed through a Drexel flask into a glass vessel filled with water. Water ejected by the gas dropped into a flask placed onto scales (ATL-8200d1-I; 'Acculab Sartorius Group', New York, NY, USA), which readings were transmitted to a computer. The temperatures in the reactor and glass vessel were measured correspondingly with an L-type thermocouple (TP.KhK(L)-K11; 'Relsib' LLC, Novosibirsk, Russia) and a Pt100-type resistance temperature detector (TS-1288 F/11; 'Elemer' LLC, Podolsk, Russia) connected to a multichannel thermometer (TM 5103; 'Elemer' LLC, Podolsk, Russia). The atmosphere pressure values were obtained using a barometer (BTKSN-18; Technical Specification No. 1-099-20-85, 'UTYOS' JSC, Ulyanovsk, Russia). The collected data were used for the calculation of hydrogen volume values at standard conditions (Standard DIN 1343: 101,325 Pa, 0 °C) in accordance with the ideal gas law. The effect of various solutions was evaluated from single experiments. And for the selected solution, all Al-based samples (with copper additives of different dispersity and without it) were tested for three times (repeated experiments).

The original materials, ball milled samples, and solid reaction product were investigated via X-ray diffraction (XRD) analysis performed at a 'Difraey 401' diffractometer ('Scientific Instruments' JSC, Saint Petersburg, Russia) with Cr-Kα radiation (0.22909 nm). The XRD patterns were processed using a database (Powder Diffraction File™) from the International Centre for Diffraction Data (ICDD). Microstructure of the samples was analyzed by scanning electron microscopy (SEM) method and included imaging in secondary electron (SE) and backscattered electron (BSE) modes. And elemental composition of the samples was evaluated by energy-dispersive X-ray spectroscopy (EDX) method. SEM-EDX analysis was performed by scanning electron microscope TESCAN VEGA3 ('Oxford Instruments' PLC, Abingdon, United Kingdom). Visual investigation and particle size measurements of the original materials and manufactured powder samples were performed using a Bio 6 model optical microscope with a high-resolution camera (UCMOS 10000KPA; 'Altami' LLC, Saint Petersburg, Russia). Particle size measurements were carried out by means of 'Altami Studio' software (version 3.5, 'Altami' LLC, Saint Petersburg, Russia). The image processing procedure included 'capturing' particles in the image by adjusting rendering settings, their contouring, and further automatic calculation of the contour sizes (maximum Feret diameters) using the calibration data.

3. Results and Discussion

3.1. Effect of Ball Milling Conditions on Phase Transformations and Dispersity of the Resulting Composites

The general view photographs of the starting materials under magnification with the corresponding particle size distributions (excepting scrap composed of large ~1–10 mm pieces) are given In Figure A1 (see Appendix A). As it can be seen, scrap shavings had a plenty of mechanical damages on their surfaces and edges, and copper particles had irregular shape and uneven surface. As to the actual sizes of the powders, the evaluated results differed from those claimed by the manufacturers; that can be ascribed to relatively small numbers of particles for averaging, deviations from the actual particle sizes caused by image processing (especially for small particles), and high divergency in the particles' sizes.

To evaluate the effect of balls' size and milling duration on phase transformations and particle size reduction of the resulting composites, eight samples of aluminum scrap and 10 wt.% copper powder PMS-1 (50–70 μm) were manufactured. Two compositions were

milled for 2 h with 5 mm balls in two different modes: continuous unidirectional rotation, and bidirectional rotation. Another two samples were mechanically activated during 1 h with 7 steel balls 15 mm in diameter, under the same two milling modes. And the last four test materials were manufactured by milling for 1 and 2 h, under the same two milling modes each, using 24 steel balls 10 mm in diameter. The images of the said samples under magnification are represented in Figure A2 (see Appendix A). It was clearly established that milling with the smallest balls resulted in the poorest particle size reduction (resulting flakes could hardly be classified as powder). The dispersity of the sample activated with the medium balls for 1 h was higher (it contained powder-like pieces and larger ones). The finest powder was obtained for 2 h ball milling with the medium balls. And the second-finest composite corresponded to 1 h activation with the largest balls. Implementation of a unidireactional rotation mode increased the share of smaller particles as compared with a less intensive bidirectional mode. However, in general, no significant difference in the particle sizes for the samples obtained under the said two modes was observed.

The phase compositions of the resulting samples were studied via XRD analysis. Their XRD patterns are represented in Figure 1. In accordance with the results, for both rotation modes, Al-Cu composition ball milled for 2 h with 5 mm steel balls included the original Al and Cu phases, Al_2Cu and Cu_9Al_4 intermetallides, and Al_2O_3 compound apparently formed by the partial Al oxidation with residual oxygen. Moreover, as it was mentioned, those milling parameters provided the worst particle size reduction of the base scrap, yielding large flakes. Milling for 2 h with 10 mm balls resulted in the best particle size reduction, effective for obtaining powders. However, the sample ball milled with a pause was composed of Al, Cu_9Al_4, and Al_2O_3 phases, and the sample milled with no pause had Al_2Cu phase as well. For those samples Cu was not detected. Under both rotation modes, the composites activated for 1 h using 10 mm balls contained Al, Cu, Cu_9Al_4, and Al_2O_3. For them particle size reduction appeared to be worse than that for 2 h milling with balls of the same size, but better than that for 2 h activation with the smaller balls. And under both rotation modes, the composites manufactured for 1 h with 15 mm balls contained the original Al and Cu phases with some amount of Al_2O_3. So, for the latest two samples, no intermetallic phases were detected, and particle size reduction was comparable with the best result (2 h, medium size balls, no pauses). Thus, the process parameters including activation with the big balls for 1 h and milling with no pauses provided the beneficial combination of effective particle size reduction and 'conservation' of the original Al and Cu phases (excepting Al_2O_3 formation apparently caused by insufficient purging with argon).

3.2. Effect of Solution Composition on Hydrogen Evolution

For all 2 M salt solutions, reaction was carried out at 60 °C. All chlorine solutions were tested at least for 50 min to access the general dynamics of the reaction process. The tested samples were composed of Al scrap activated with 10 wt.% of PMS-1 powder ball milled for 1 h with 15 mm steel balls in a unidirectional rotation mode with no pauses. The resulting hydrogen yield kinetic curves are shown in Figure 2. The results demonstrated that under the tested conditions (salt concentrations, temperature, and sample preparation method) NaCl, KCl, LiCl, $BaCl_2$, $ZnCl_2$, and $MgCl_2$ solutions appeared to be almost useless for hydrogen generation, providing hydrogen yield below 4%. $NiCl_2$ and $CaCl_2$ demonstrated first- and second-highest reaction rates at the beginning; $FeCl_2$ and $CoCl_2$ started their reactions with the samples relatively fast. For $CaCl_2$ solution, the reaction decayed rather soon after such a promising beginning. In cases of Ni, Fe, and Co chlorides, metal pieces anchored to the magnetic stirring bar were observed, that indicated proceeding of another parallel exchange reaction between Al and the salts of those metals. Such a reaction promoted hydrogen release, but at the same time obviously consumed a considerable amount of aluminum.

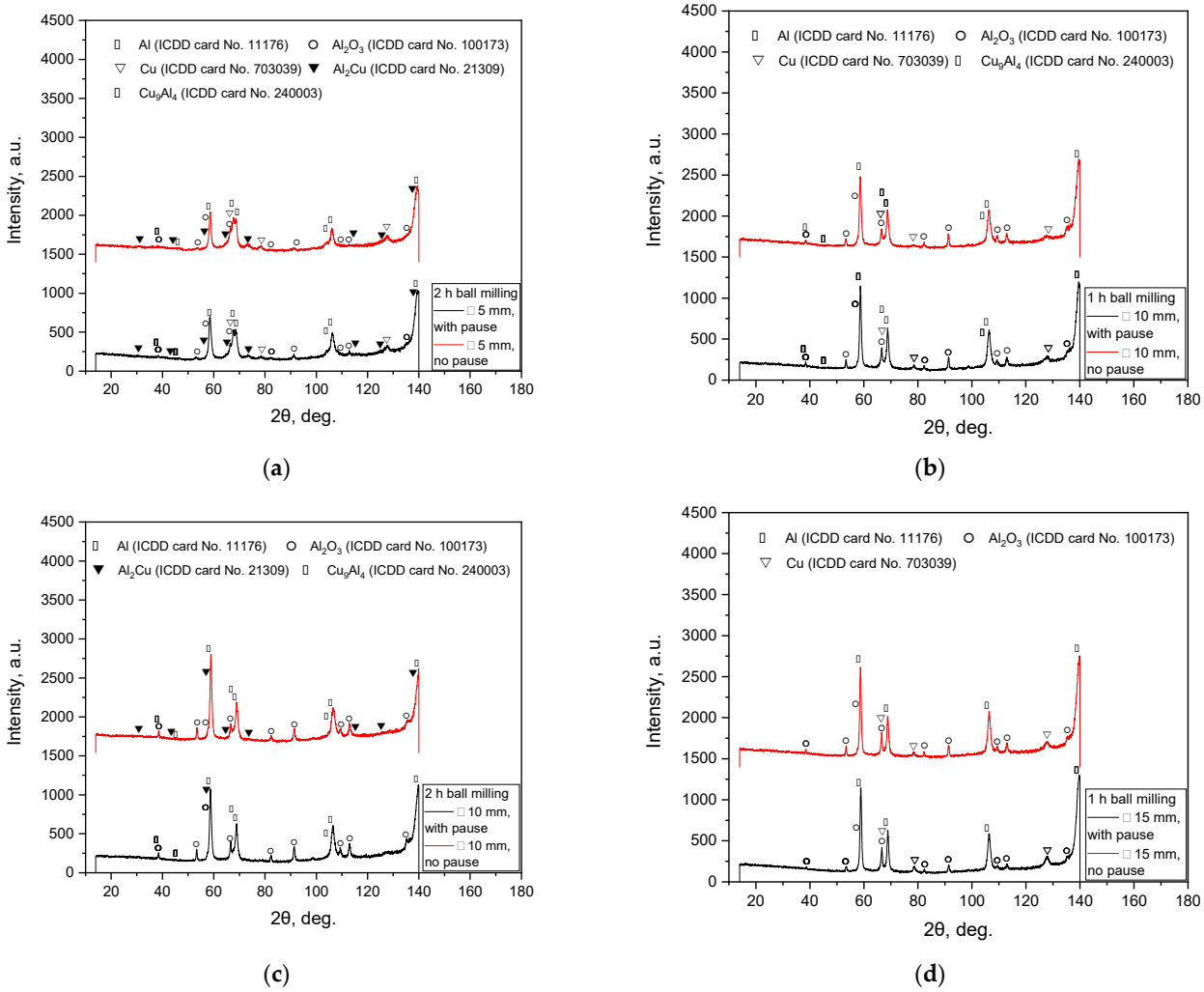


Figure 1. XRD patterns of the samples with different ball milling parameters: (**a**) 2 h, 5 mm steel balls; (**b**) 1 h, 10 mm steel balls; (**c**) 2 h, 10 mm steel balls; (**d**) 1 h, 15 mm steel balls.

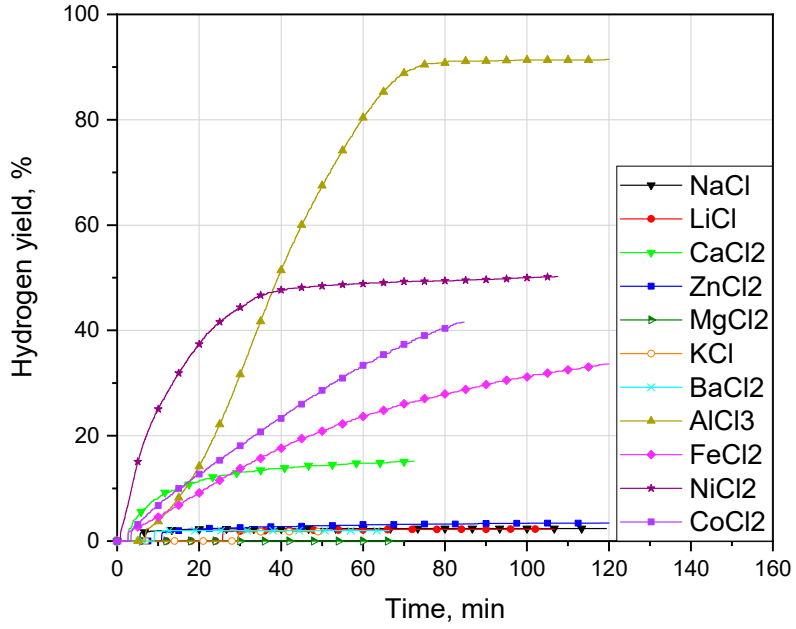


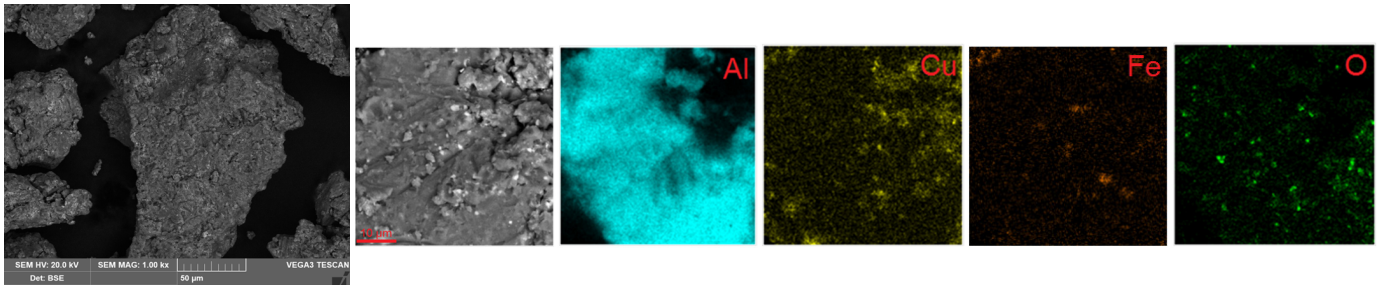
Figure 2. Hydrogen yield kinetic curves for different solution compositions.

As to $AlCl_3$ solution, the corresponding kinetic curve had a clear S-shape, typical for topochemical reactions, with the acceleration region in the beginning, section with the maximum reaction rate and deceleration, and termination part [101]. That solution provided the highest hydrogen yield of 91.5%. The value fell below 100% due to a partial oxidation of the scrap with residual oxygen during ball milling, which was proved by the XRD results. The effect of $AlCl_3$ constituted in its transformation, by hydrolysis, into high soluble complexes: $Al(H_2O)_6^{3+}$ (pH < 3.6), $[Al(OH)(H_2O)_4]^{2+}$ and $[Al(OH)_2(H2O)_2]^{+}$ (pH ~4), $[Al(OH)(H_2O)_4]^{2+}$ and $[Al(OH)_4]^{-}$ (5.2 < pH < 6.7), and $[Al(OH)_4]^{-}$ (pH > 7.0) [102,103]. The filtered reaction product did not contain any solids looking like boehmite or aluminum hydroxide. The apparent reason for that was the formation of soluble aluminum compounds instead of poorly soluble dense layers of AlOOH or $Al(OH)_3$. The pH value of 2 M $AlCl_3$ solution measured at 25 °C with a Multiparameter Transmitter M300 (JSC 'Mettler Toledo', Greifensee, Switzerland) was ~1.25. So, according to the above data, the measured pH corresponds to $Al(H_2O)_6^{3+}$ soluble compound. The resulting dehydrated solid product from the interaction between Al and hydrolyzed $AlCl_3$ solution represents a hydroxychloride compound $Al_m(OH)_nCl_{3m-n}$ ($m \geq 1$; $0 < n \leq 3m$). The basicity of the polyaluminum chloride is defined as n/3m, and the highest basicity of ~83% corresponds to $Al_2(OH)_5Cl{\cdot}2H_2O$. Lesukite ($Al_2(OH)_5Cl{\cdot}2H_2O$) is a useful material for water treatment and for binding of antibacterial agents to cotton fabric [104–106]. As reported in [107], under thermal treatment at 543 K, $Al_2(OH)_5Cl$ transforms into $Al(OH)_2Cl$, AlOOH, and H_2O (and at 723 K, $Al(OH)_2Cl$ decomposes into Al_2O_3, HCl, and H_2O). So, in theory, aluminum oxidized with $AlCl_3$ solution can be recovered by AlOOH dehydration and electrolysis of Al_2O_3.

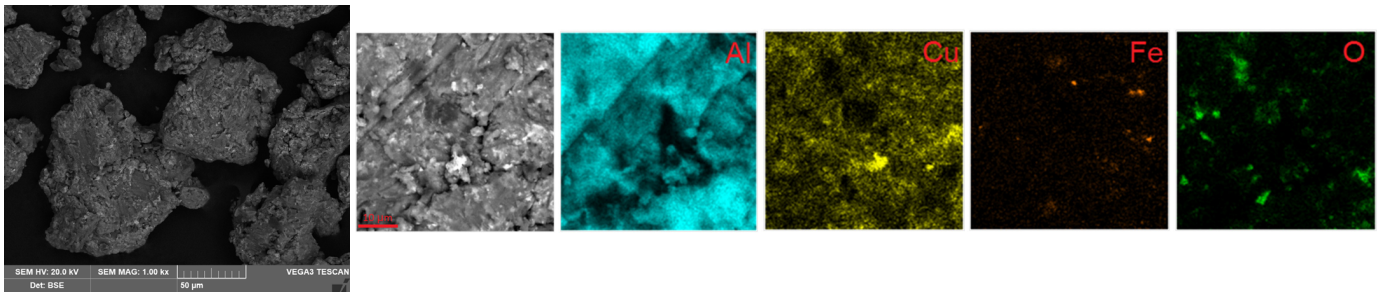
3.3. Effect of Copper Powder Particle Size

To investigate the effects of copper particle size as well as its substantive presence, four samples containing 10 wt.% additive of 50–100 nm, 1–19 μm, 50–70 μm, and 150–250 μm powders, and a sample ball milled with no additive, were manufactured. The activation process parameters were 1 h, unidirectional ball milling (no pauses), 15 mm steel balls. Due to the detection of aluminum oxide in the previously described samples, more intensive argon purging of the glove box was executed. The composites' photographs under magnification are given in Figure A2 (see Appendix A). No any visible differences between the samples were detected. Also the five samples were investigated by SEM and EDX methods, and the respective visual data are represented in Figure 3.

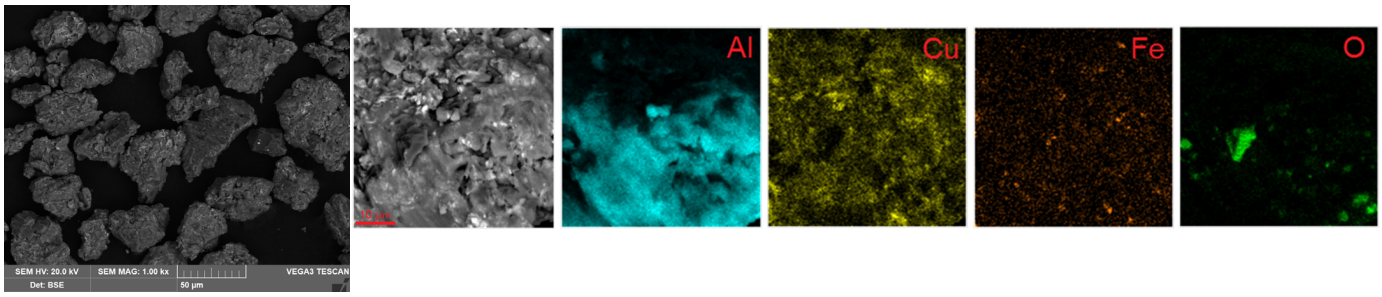
In the SEM images (BSE mode) of the samples modified with copper powders, the basic aluminum was shown in dark-grey, and copper were illustrated by white and light-grey dots and spots with sharp or blurry contours. The mentioned copper-rich regions did not have any drastic differences in sizes, excepting those for the sample with 150–250 μm powder were somewhat larger, and those for 50–100 nm were generally smaller. The SEM image of the sample without copper powder (BSE mode) did not show any considerable contrast areas. And its microstructure, captured under SE mode, was similar to the microstructure of all four other samples milled with powders. As it can be seen, the particles represented solid shape structures formed by agglomerated smaller metal pieces. As it can be expected, 1 h ball milling with 15 mm balls (with no pauses) resulted in shear tearing as well as deformation embrittlement and fracturing of the original chips and shavings (several mm in size) into small pieces which agglomerated by cold welding. Large copper particles likely reduced their sizes, while small ones, in contrast, agglomerated. Then they were cold welded to aluminum particles, and some of them got smeared over the surface. Presumably, some of the copper particles got embedded beneath the surface because of the said 'disintegration and integration' processes of the scrap particles structural evolution.



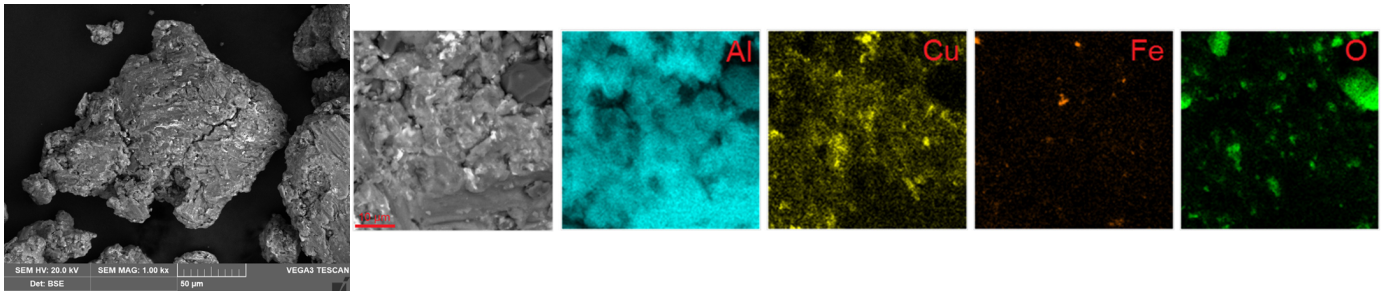
(**a**)



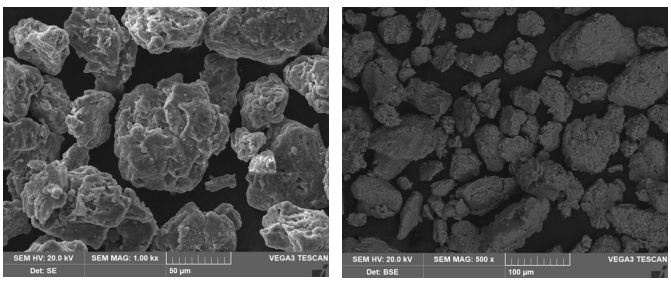
(**b**)



(**c**)



(**d**)



(**e**)

Figure 3. SEM images and the corresponding EDX element distribution maps for different ball milled samples: (**a**) 50–100 nm copper powder; (**b**) 1–19 µm copper powder; (**c**) 50–70 µm copper powder; (**d**) 150–250 µm copper powder; (**e**) without copper powder.

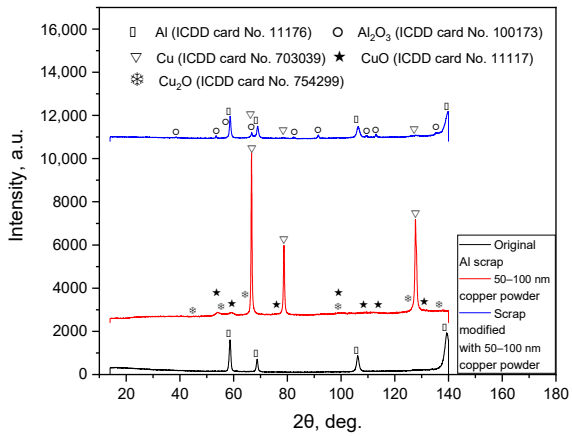
The EDX analyses for the samples mechanically activated with copper powders evidenced the presence of Al (basic phase), Cu, Mg, and Mn—alloying elements; some amount of Fe likely represented one more of the alloying elements, while the rest, together with C, could be contamination from steel balls. The element distribution maps illustrate the most important components of the composite samples. Unfortunately, despite more intensive purging with Ar, for all samples O, apparently resulting from the aluminum interaction with residual oxygen under high energy milling, was detected. That could point to the imperfection of the used procedure for filling the milling pot with the original samples and balls in the glove box. Probably, to prevent the undesired oxidation, a special lid modification (with intake and exhaust nozzles for direct purging with protective gas), or wet milling in a protective liquid, should be used. From the comparison between the images for Cu and O distributions, it can be established that for the visible surface of the particle with 50–100 nm Cu powder, O distribution was generally more uniform, while Cu-rich regions were less dense, as compared to the other composites.

The XRD patterns of the original materials, ball milled samples, and filtered solid product (from the reaction of scrap modified with 50–70 μm copper powder with 2 M $AlCl_3$ solution), are given in Figure 4. The results proved that in addition to the basic Cu phase, Cu nanopowder initially contained Cu_2O and CuO phases as well. Apparently, intensive oxidation by air is a common case for Cu nanopowders. Another small sized powder (1–19 μm), besides Cu, also contained Cu_2O phase. For both larger powders (50–70 and 150–250 μm), single Cu phase was detected.

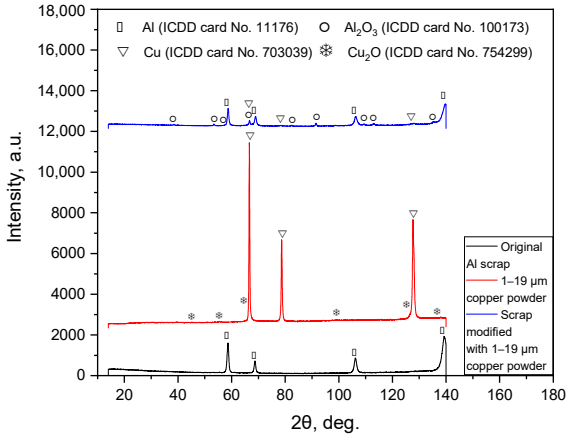
For the original scrap, only Al phase was identified by XRD analysis. In more detail, its composition was evaluated by EDX measurements of its sample, ball milled for 1 h without copper powder. According to the elemental composition assessment, the scrap, milled as it was, contained (92.51 ± 0.49) wt.% Al, (1.69 ± 0.52) wt.% Mg, (0.71 ± 0.10) wt.% Mn, (4.74 ± 0.63) wt.% Cu, and (0.44 ± 0.14) wt.% Fe. The obtained values match the corresponding elemental contents of D16 grade alloy. The possible reason of the alloying elements 'invisibility' for XRD analysis was the potential presence of intermetallic phases Al_2CuMg, Al_2Cu, and existing of Guinier–Preston zones (enriched with copper) typical for aged dural alloys. So, the main alloying element (Cu) could be distributed among different phases, and each of those phases could present in a negligible amount.

The solid residuals, remaining after the reaction, were examined with the optical microscope in a dark field mode. The respective images (and particle size distributions) are shown in Figure A3 (see Appendix A). The residuals majorly represented fine copper pieces with some amount of larger ones. The solids remaining from the sample of 100% scrap, apparently, represented copper (or enriched with copper) component of the D16 aluminum alloy; as compared to the composite samples, its amount was insignificant. Aside from the obvious size difference between the largest copper fractions, no explicit variance in the sizes of the most abundant fine fractions was detected.

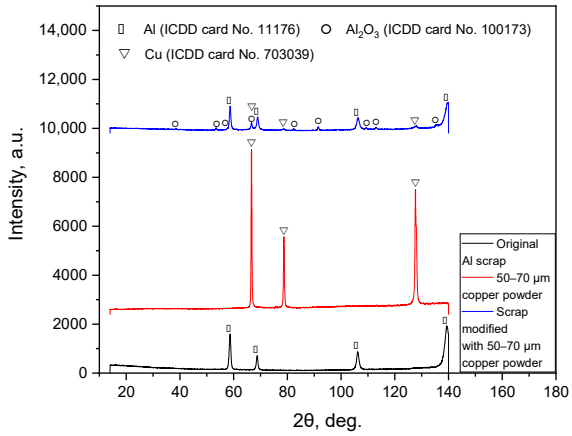
The sample of the scrap ball milled without copper additive contained Al and Al_2O_3 phases. And for all composites with different copper powders, Al, Cu, and Al_2O_3 were identified. A closer visual examination of the Al_2O_3 peaks revealed that majorly those for the sample with nanopowder and without additive were the largest and smallest, respectively, while for the rest of the composites they had similar sizes. The filtered solid reaction product contained Cu, Cu_2O, and Al_2O_3 phases, with the latest two apparently resulting from the reaction and ball milling respectively. As it was assumed earlier, none of Al, $Al(OH)_3$, or AlOOH were 'found' in the product. Thus, Al reacted with $AlCl_3$ solution with the formation of water-soluble compounds.



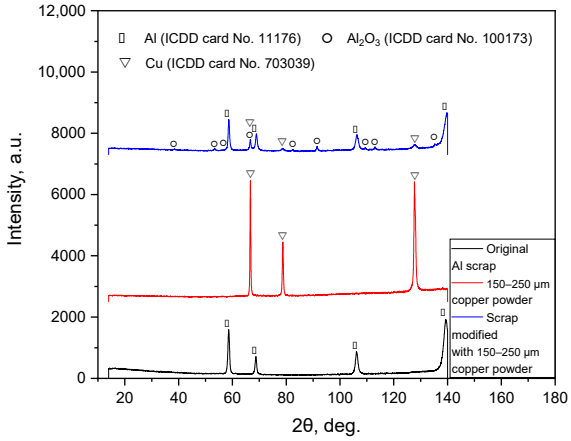
(**a**)



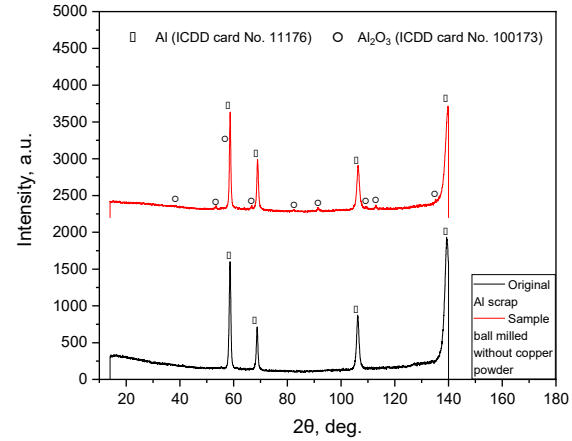
(**b**)



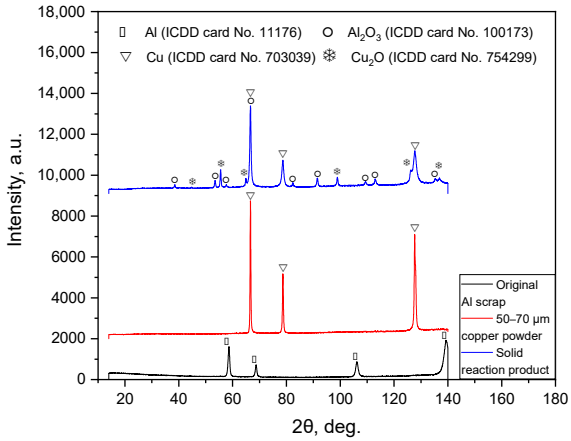
(**c**)



(**d**)



(**e**)



(**f**)

Figure 4. XRD patterns of the original materials, ball milled samples modified with different copper powders, sample ball milled as it was, and filtered solid reaction product: (**a**) 50–100 nm copper powder; (**b**) 1–19 μm copper powder; (**c**) 50–70 μm copper powder; (**d**) 150–250 μm copper powder; (**e**) without copper powder; (**f**) reaction product (from scrap and 50–70 μm copper powder composite).

Figure 5 illustrates the effect of scrap modification with copper powders with various particle sizes. As it can be seen, the kinetic curves for the samples ball milled with different powders and without additive had their error bars overlapping at the beginning and termination stages of the reaction. However, in the interval from nearly 40 to 60 min, the curves clearly deviated from each other. There were several time intervals containing gaps between the error bars of different hydrogen yield kinetic curves. The existence of the said gaps proved that the reaction kinetics was affected by the presence of copper powders and their dispersity.

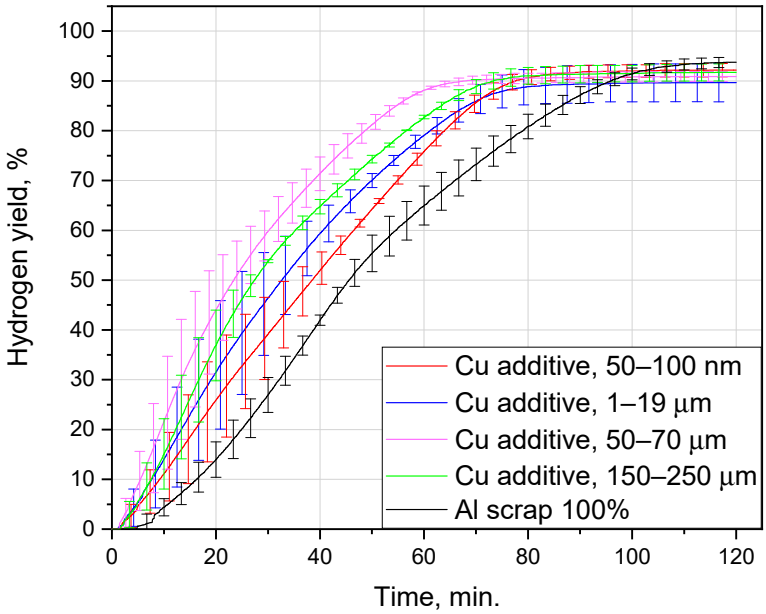


Figure 5. Hydrogen yield kinetic curves for the samples with different copper powder sizes and one ball milled without copper.

The resulting hydrogen yields and maximum hydrogen evolution rates are listed in Table 1. For all samples, their total hydrogen yields achieved close values falling within the range ~90–94%. The missing hydrogen was attributed to the abovementioned partial oxidation of Al during ball milling.

Table 1. Hydrogen production yields and rates for different samples.

Sample	Maximum H_2 Evolution Rate, mL/min/g	H_2 Yield,%
Scrap and Cu additive (50–100 nm)	26.4 ± 3.4	92.18 ± 1.33
Scrap and Cu additive (1–19 μm)	33.7 ± 12.3	89.68 ± 3.87
Scrap and Cu additive (50–70 μm)	39.8 ± 7.0	90.90 ± 1.02
Scrap and Cu additive (150–250 μm)	35.3 ± 3.9	91.71 ± 1.71
Scrap without copper powder	27.5 ± 1.4	93.73 ± 1.06

The effect of modification with copper additive revealed itself in the accelerated reaction between Al and $AlCl_3$ solution, as compared to the unmodified sample. For the samples with additives, the reaction almost terminated after approximately 70–80 min, while for the sample of scrap only it took nearly 110 min. The maximum reaction rates for the sample with nanopowder and without additive were close to each other: (27.5 ± 1.4) and (26.4 ± 3.4) mL/min/g, respectively. The corresponding values for 50–70 and 150–250 μm modifiers definitely were larger—(39.8 ± 7.0) and (35.3 ± 3.9) mL/min/g. And that for the sample with 1–19 μm powder had a large uncertainty: (33.7 ± 12.3) mL/min/g.

The results demonstrated that under the tested experimental conditions (original materials, sample compositions, ball milling parameters, selected salt solution and temperature), the fastest scrap utilization with hydrogen evolution was provided via the sample modified with 50–70 μm powder. The second- and third-highest rates corresponded respectively to 150–250 and 1–19 μm copper additives. And the first- and second-lowest results were obtained correspondingly for 50–100 nm modifier and scrap with no additive. The slowest process for the sample without additive apparently was caused by the lack of 'microgalvanic cells' between Cu and Al phases promoting galvanic corrosion with hydrogen evolution. And the lowest activation result for nanopowder can be ascribed to the presence of copper oxides in it, more uniform distribution of O over the surface and slightly higher content of Al_2O_3, and lower density of Cu distributed over the surface, which could delay the reaction process at the beginning. As to the other three samples, the highest performance for the 50–70 μm powder possibly could be associated with the most profitable Cu distribution in the sample during ball milling, as compared with the finer and coarser powders.

4. Conclusions

In the present study, complex effects of oxidation medium, ball milling parameters, and copper powder dispersity on the oxidation of aluminum scrap with hydrogen evolution were studied. The key findings of the study were the following ones:

- variations in ball milling parameters resulted in different phase compositions and particle sizes of the composite samples—after 2 h of activation, the smallest milling balls provided the worst particle size reduction and formation of as much as three new phases, Al_2Cu, Cu_9Al_4, and Al_2O_3, besides the original Al and Cu. After 2 h milling with medium-sized balls, Cu disappeared, detected phases were Al_2Cu, Cu_9Al_4, Al, and Al_2O_3, and the finest powder was obtained. Activation for 1 h with medium-sized balls added Cu_9Al_4, and Al_2O_3 compounds to the original Al and Cu, and reduced particle sizes to the values falling between the mentioned two. And activation with the largest balls for 1 h provided the best 'conservation' of the original phase composition (Al, Cu, and some Al_2O_3) and the second-smallest particle sizes;
- among the tested chlorine solutions, the least impressive results were obtained for NaCl, KCl, LiCl, $BaCl_2$, $ZnCl_2$, and $MgCl_2$ solutions. Somewhat better performance corresponded to $CaCl_2$, $NiCl_2$, $CoCl_2$, and $FeCl_2$ apparently interacting with Al via an exchange reaction, thus consuming some of its amount while promoting its intended reaction with hydrogen production. The highest result of 91.5% hydrogen yield was obtained for $AlCl_3$ solution. Neither Al, nor any Al-based compounds (excepting initially presenting Al_2O_3) were detected in the filtered solid reaction products, because Al reaction with $AlCl_3$ led to the formation of water soluble compounds;
- after 2 h of experiment, all samples eventually yielded almost the same amounts of hydrogen (~90–94%), but their reaction rates differed. The lowest rates corresponded to the samples of 100% scrap and with 50–100 nm copper powder. In the first case, the reason was the lack of Cu-Al couples promoting galvanic corrosion in conductive media ($AlCl_3$ solution). In the second case, reaction delaying at the beginning was presumably caused by the presence of copper oxides, more uniform distribution of O over the particles' surface, slightly higher content of Al_2O_3, and lower Cu distribution density. The highest rate for the sample with 50–70 μm Cu powder was presumably ascribed to the fact that the Cu distribution density and sizes of copper-enriched sites appeared to be optimal (as compared with coarser and finer additives), with its 'cathodic' structure effectively promoting Al corrosion with hydrogen generation.

Author Contributions: Conceptualization, methodology, investigation, formal analysis, funding acquisition, writing—original draft preparation, O.A.B.; data curation, visualization, M.Z.S.; validation, supervision, V.K. and G.N.A.; writing—review and editing, resources, project administration, M.S.V. All authors have read and agreed to the published version of the manuscript.

Funding: This work was funded by the Russian Science Foundation (RSF), Grant No. 22-29-01384, https://rscf.ru/en/project/22-29-01384/ (accessed on 22 November 2022).

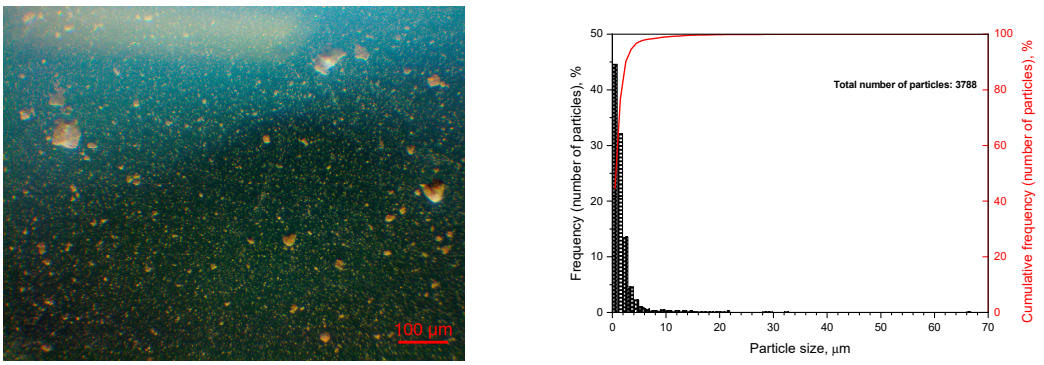
Data Availability Statement: Not applicable.

Acknowledgments: We would like to express our gratitude to the Russian Science Foundation (RSF) for funding the present research project (Grant No. 22-29-01384, https://rscf.ru/en/project/22-29-01384/, accessed on 22 November 2022).

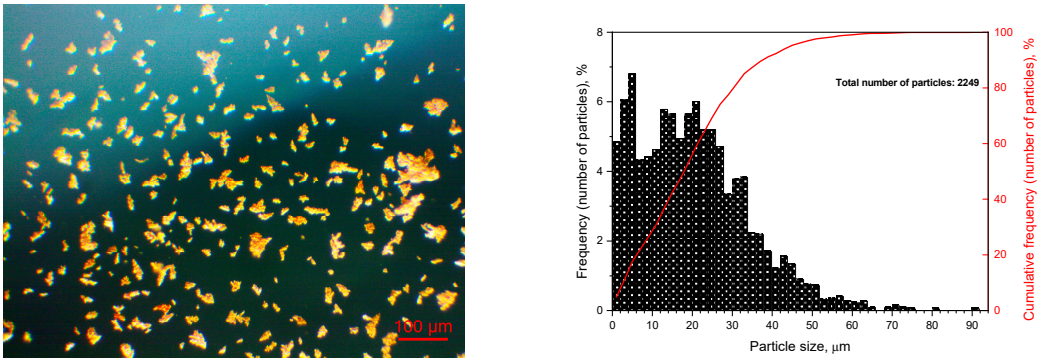
Conflicts of Interest: The authors declare no conflict of interest.

Appendix A

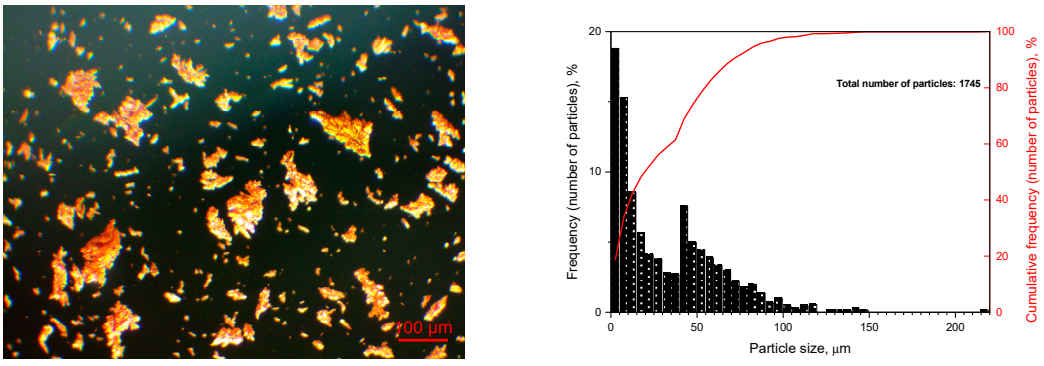
The images and particle size distributions (histograms and cumulative curves) for the original materials, composite samples and solid reaction product residuals are represented in Figures A1–A3.



(**a**)

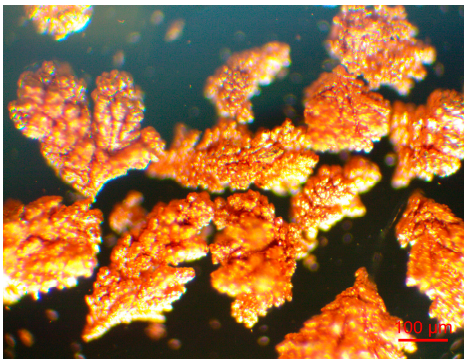


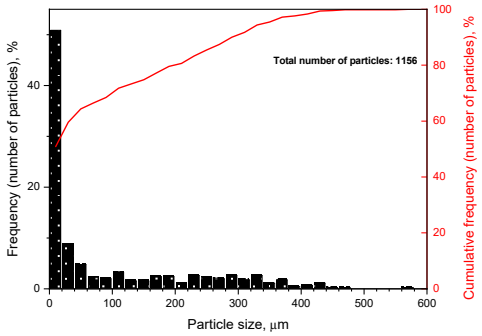
(**b**)



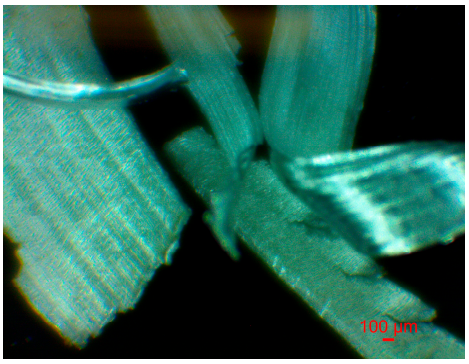
(**c**)

Figure A1. *Cont.*



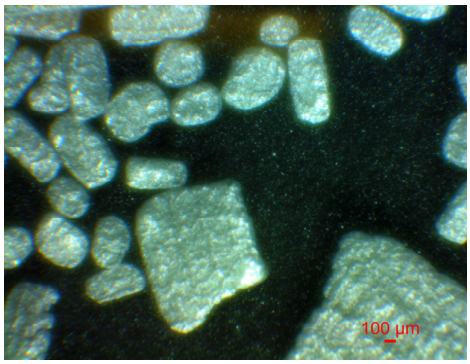


(**d**)

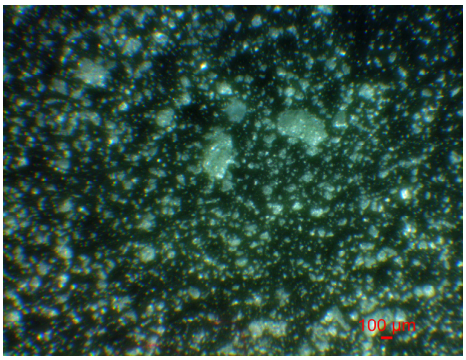


(**e**)

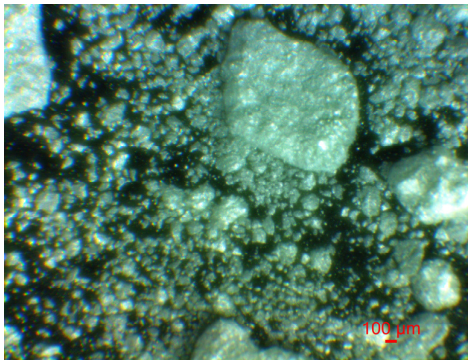
Figure A1. Optical microscope images and particle size distributions for original materials: (**a**) 50–100 nm copper powder; (**b**) 1–19 µm copper powder; (**c**) 50–70 µm copper powder; (**d**) 150–250 µm copper powder; (**e**) original aluminum-based scrap.



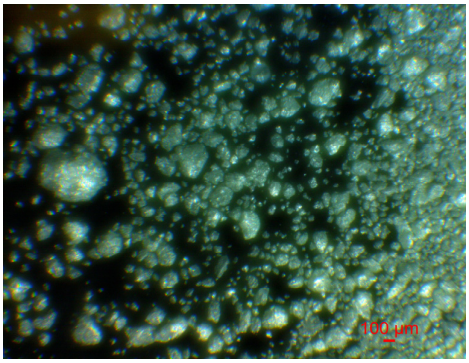
(**a**)



(**b**)

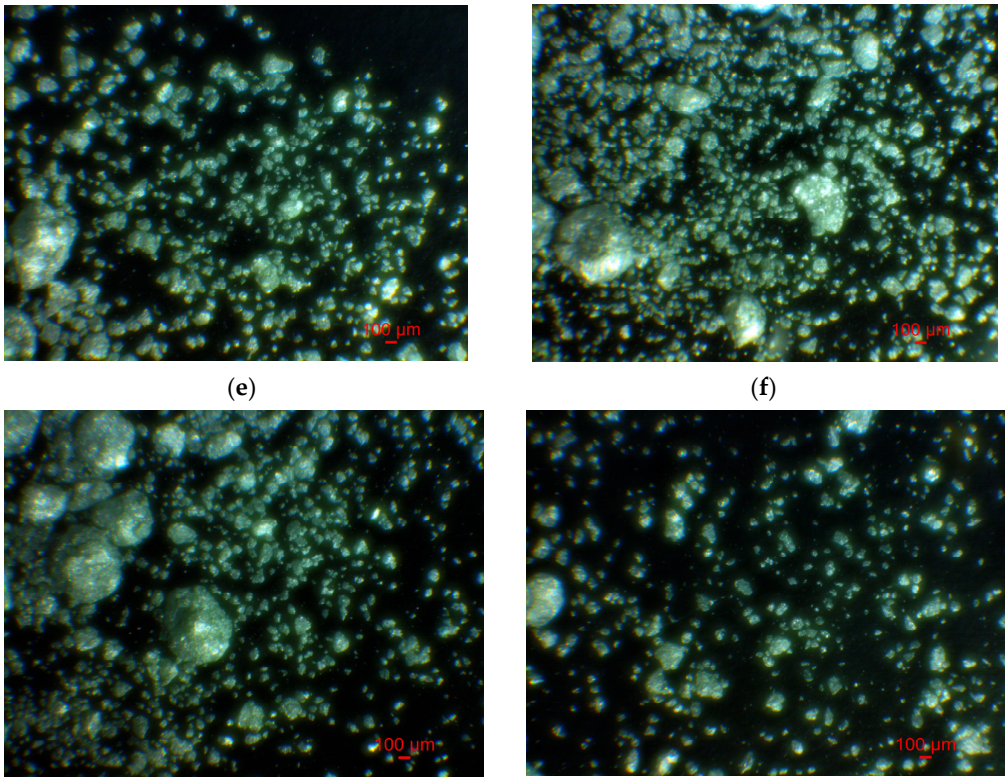


(**c**)



(**d**)

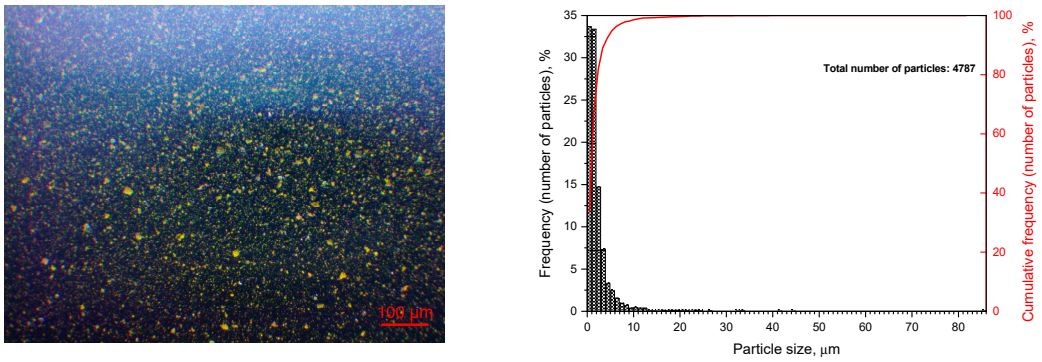
Figure A2. *Cont.*



(**e**) (**f**)

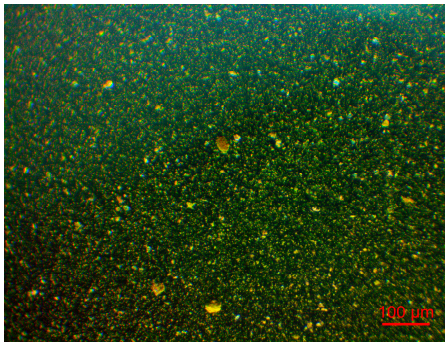
(**g**) (**h**)

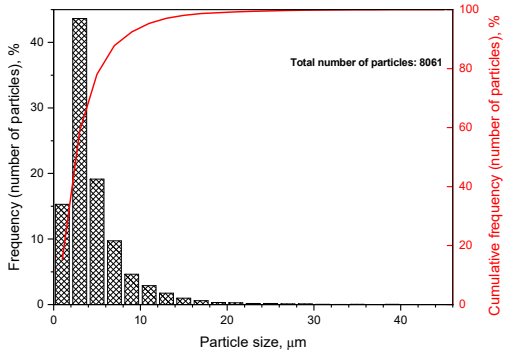
Figure A2. Optical microscope images of scrap and copper composites ball milled at different conditions: (**a**) 50–70 µm copper powder, 2 h, 5 mm steel balls; (**b**) 50–70 µm copper powder, 2 h, 10 mm steel balls; (**c**) 50–70 µm copper powder, 1 h, 10 mm steel balls; (**d**) 50–70 µm copper powder, 1 h, 15 mm steel balls; (**e**) 50–100 nm copper powder, 1 h, 15 mm steel balls; (**f**) 1–19 µm copper powder, 1 h, 15 mm steel balls; (**g**) 150–250 µm copper powder, 1 h, 15 mm steel balls; (**h**) no copper powder, 1 h, 15 mm steel balls.



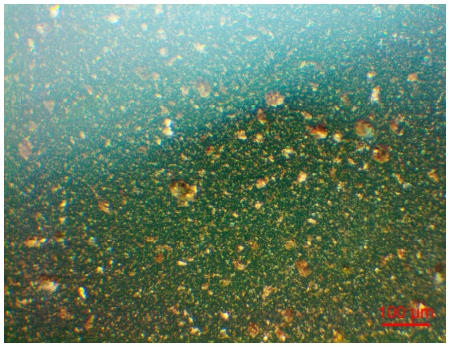
(**a**)

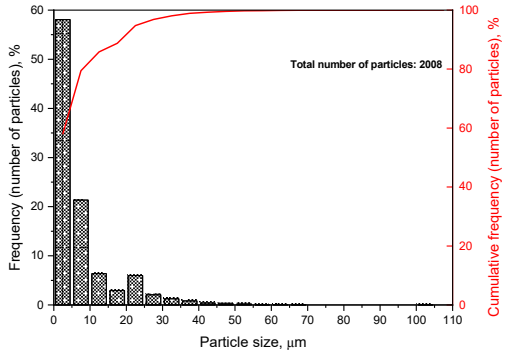
Figure A3. *Cont.*



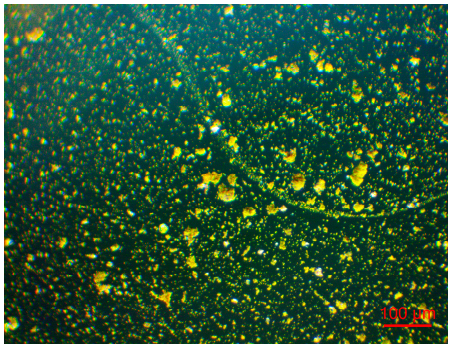


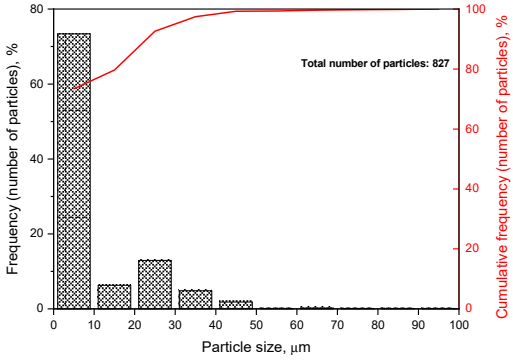
(**b**)





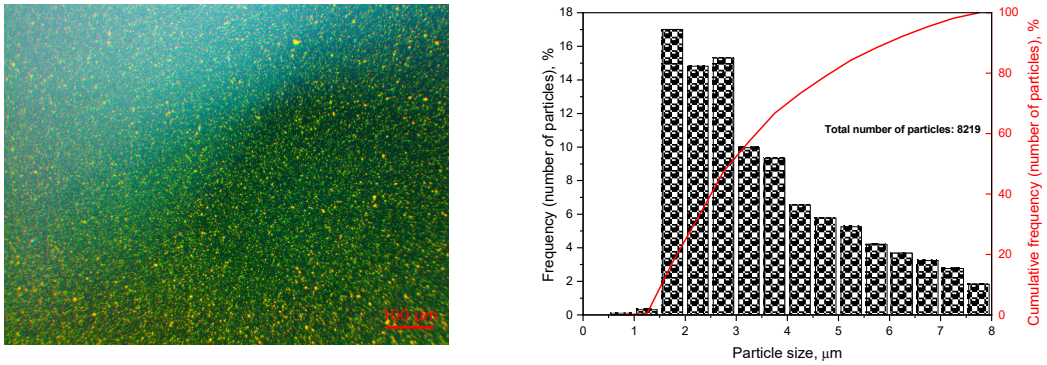
(**c**)





(**d**)

Figure A3. *Cont.*



(**e**)

Figure A3. Optical microscope images and particle size distributions for solid residuals remaining after reaction of different composite samples: (**a**) scrap and 50–100 nm copper powder; (**b**) scrap and 1–19 μm copper powder; (**c**) scrap and 50–70 μm copper powder; (**d**) scrap and 150–250 μm copper powder; (**e**) scrap ball milled without additives (copper contained in D16 aluminum alloy).

References

1. Koukouzas, N.; Christopoulou, M.; Giannakopoulou, P.P.; Rogkala, A.; Gianni, E.; Karkalis, C.; Pyrgaki, K.; Krassakis, P.; Koutsovitis, P.; Panagiotaras, D.; et al. Current CO_2 Capture and Storage Trends in Europe in a View of Social Knowledge and Acceptance. A Short Review. *Energies* **2022**, *15*, 5716. [CrossRef]
2. Chu, W.; Vicidomini, M.; Calise, F.; Duić, N.; Østergaard, P.A.; Wang, Q.; da Graça Carvalho, M. Recent Advances in Low-Carbon and Sustainable, Efficient Technology: Strategies and Applications. *Energies* **2022**, *15*, 2954. [CrossRef]
3. Sadhukhan, J. Net-Zero Action Recommendations for Scope 3 Emission Mitigation Using Life Cycle Assessment. *Energies* **2022**, *15*, 5522. [CrossRef]
4. Sulich, A.; Sołoducho-Pelc, L. Changes in Energy Sector Strategies: A Literature Review. *Energies* **2022**, *15*, 7068. [CrossRef]
5. Hammond, G.P.; Titley, A.A. Small-Scale Combined Heat and Power Systems: The Prospects for a Distributed Micro-Generator in the ‘Net-Zero’ Transition within the UK. *Energies* **2022**, *15*, 6049.
6. Khan, A.A.; Minai, A.F.; Pachauri, R.K.; Malik, H. Optimal Sizing, Control, and Management Strategies for Hybrid Renewable Energy Systems: A Comprehensive Review. *Energies* **2022**, *15*, 6249. [CrossRef]
7. Issa, M.; Ilinca, A.; Martini, F. Ship Energy Efficiency and Maritime Sector Initiatives to Reduce Carbon Emissions. *Energies* **2022**, *15*, 7910. [CrossRef]
8. Vodovozov, V.; Raud, Z.; Petlenkov, E. Review of Energy Challenges and Horizons of Hydrogen City Buses. *Energies* **2022**, *15*, 6945. [CrossRef]
9. Meena, C.S.; Kumar, A.; Jain, S.; Rehman, A.U.; Mishra, S.; Sharma, N.K.; Bajaj, M.; Shafiq, M.; Eldin, E.T. Innovation in Green Building Sector for Sustainable Future. *Energies* **2022**, *15*, 6631. [CrossRef]
10. Arellano-Prieto, Y.; Chavez-Panduro, E.; Salvo Rossi, P.; Finotti, F. Energy Storage Solutions for Offshore Applications. *Energies* **2022**, *15*, 6153. [CrossRef]
11. Ravi, S.S.; Aziz, M. Utilization of Electric Vehicles for Vehicle-to-Grid Services: Progress and Perspectives. *Energies* **2022**, *15*, 589. [CrossRef]
12. Sharma, S.; Agarwal, S.; Jain, A. Significance of Hydrogen as Economic and Environmentally Friendly Fuel. *Energies* **2021**, *14*, 7389. [CrossRef]
13. Kanwal, F.; Torriero, A.A.J. Biohydrogen—A Green Fuel for Sustainable Energy Solutions. *Energies* **2022**, *15*, 7783.
14. Badea, G.E.; Hora, C.; Maior, I.; Cojocaru, A.; Secui, C.; Filip, S.M.; Dan, F.C. Sustainable Hydrogen Production from Seawater Electrolysis: Through Fundamental Electrochemical Principles to the Most Recent Development. *Energies* **2022**, *15*, 8560. [CrossRef]
15. Miyagawa, T.; Goto, M. Hydrogen Production Cost Forecasts since the 1970s and Implications for Technological Development. *Energies* **2022**, *15*, 4375. [CrossRef]
16. Osman, A.I.; Mehta, N.; Elgarahy, A.M.; Hefny, M.; Al-Hinai, A.; Al-Muhtaseb, A.H.; Rooney, D.W. Hydrogen production, storage, utilisation and environmental impacts: A review. *Environ. Chem. Lett.* **2022**, *20*, 153–188. [CrossRef]
17. Huang, Y.; Wang, Z.; Shen, S.; Huang, L.; Zhong, W.; Pan, J.; Li, C. Double-walled carbon nanotube assisted phase engineering in CoOxSy complexes for efficient oxygen evolution reaction. *CrystEngComm* **2022**, *24*, 4857–4863. [CrossRef]
18. Zhang, L.; Wang, Z.; Zhang, J.; Lin, Z.; Zhang, Q.; Zhong, W.; Wu, G. High activity and stability in Ni2P/(Co,Ni)OOH heterointerface with a multiple-hierarchy structure for alkaline hydrogen evolution reaction. *Nano Res.* **2022**. [CrossRef]

19. Olabi, A.G.; Bahri, A.S.; Abdelghafar, A.A.; Baroutaji, A.; Sayed, E.T.; Alami, A.H.; Rezk, H.; Abdelkareem, M.A. Large-vscale hydrogen production and storage technologies: Current status and future directions. *Int. J. Hydrogen Energy* **2021**, *46*, 23498–23528. [CrossRef]
20. Najjar, Y.S.H. Hydrogen safety: The road toward green technology. *Int. J. Hydrogen Energy* **2013**, *38*, 10716–10728. [CrossRef]
21. Hassan, I.A.; Ramadan, H.S.; Saleh, M.A.; Hissel, D. Hydrogen storage technologies for stationary and mobile applications: Review, analysis and perspectives. *Renew. Sustain. Energy Rev.* **2021**, *149*, 111311. [CrossRef]
22. Bunker, B.C.; Nelson, G.C.; Zavadil, K.R.; Barbour, J.C.; Wall, F.D.; Sullivan, J.P.; Windisch, C.F.; Engelhardt, M.H.; Baer, D.R. Hydration of Passive Oxide Films on Aluminum. *J. Phys. Chem. B* **2002**, *106*, 4705–4713. [CrossRef]
23. Grigorenko, A.V.; Ambaryan, G.N.; Valyano, G.E.; Vlaskin, M.S.; Gromov, A.A.; Zmanovsky, S.V. Kinetics of Aluminum Micron Powder Oxidation in Hot Distilled Water and Product Microstructure Investigation. *IOP Conf. Ser. Mater. Sci. Eng.* **2018**, *381*, 012028. [CrossRef]
24. Buryakovskaya, O.A.; Vlaskin, M.S.; Grigorenko, A.V. Effect of Thermal Treatment of Aluminum Core-Shell Particles on Their Oxidation Kinetics in Water for Hydrogen Production. *Materials* **2021**, *14*, 6493. [CrossRef] [PubMed]
25. Yavor, Y.; Goroshin, S.; Bergthorson, J.M.; Frost, D.L.; Stowe, R.; Ringuette, S. Enhanced hydrogen generation from aluminum-water reactions. *Int. J. Hydrogen Energy* **2013**, *38*, 14992–15002. [CrossRef]
26. Vostrikov, A.A.; Shishkin, A.V.; Fedyaeva, O.N. Conjugated processes of bulk aluminum and hydrogen combustion in water-oxygen mixtures. *Int. J. Hydrogen Energy* **2020**, *45*, 1061–1071. [CrossRef]
27. Bersh, A.V.; Lisitsyn, A.V.; Sorokovikov, A.I.; Vlaskin, M.S.; Mazalov, Y.A.; Shkol'Nikov, E.I. Study of the Processes of Steam-Hydrogen Mixture Generation in a Reactor for Hydrothermal Aluminum Oxidation for Power Units. *High Temp.* **2010**, *48*, 866–873. [CrossRef]
28. Vlaskin, M.S.; Dudoladov, A.O.; Buryakovskaya, O.A.; Ambaryan, G.N. Modelling of aluminum-fuelled power plant with steam-hydrogen enthalpy utilization. *Int. J. Hydrogen Energy* **2018**, *43*, 4623–4631. [CrossRef]
29. Vostrikov, A.A.; Fedyaeva, O.N.; Fadeeva, I.I.; Sokol, M.Y. The formation of Al_2O_3 nanoparticles in the oxidation of aluminum by water under sub- and supercritical conditions. *Russ. J. Phys. Chem. B* **2010**, *4*, 1051–1060. [CrossRef]
30. Potapova, Y.V.; Tikhov, S.F.; Sadykov, V.A.; Fenelonov, V.B. Kinetics of aluminium powder oxidation by water vapor at moderate temperatures. *React. Kinet. Catal. Lett.* **2001**, *73*, 55–61. [CrossRef]
31. Godart, P.; Fischman, J.; Seto, K.; Hart, D. Hydrogen production from aluminum-water reactions subject to varied pressures and temperatures. *Int. J. Hydrogen Energy* **2019**, *44*, 11448–11458. [CrossRef]
32. Trowell, K.; Goroshin, S.; Frost, D.; Bergthorson, J. Hydrogen production rates of aluminum reacting with varying densities of supercritical water. *RSC Adv.* **2022**, *12*, 12335–12343. [CrossRef] [PubMed]
33. Vlaskin, M.S.; Valyano, G.E.; Zhuk, A.Z.; Shkolnikov, E.I. Oxidation of coarse aluminum in pressured water steam for energy applications. *Int. J. Energy Res.* **2020**, *44*, 8689–8715. [CrossRef]
34. Trowell, K.A.; Goroshin, S.; Frost, D.L.; Bergthorson, J.M. The use of supercritical water for the catalyst-free oxidation of coarse aluminum for hydrogen production. *Sustain. Energy Fuels* **2020**, *4*, 5628–5635. [CrossRef]
35. Alinejad, B.; Mahmoodi, K. A novel method for generating hydrogen by hydrolysis of highly activated aluminum nanoparticles in pure water. *Int. J. Hydrogen Energy* **2009**, *34*, 7934–7938. [CrossRef]
36. Mahmoodi, K.; Alinejad, B. Enhancement of hydrogen generation rate in reaction of aluminum with water. *Int. J. Hydrogen Energy* **2010**, *35*, 5227–5232. [CrossRef]
37. Skrovan, J.; Alfantazi, A.; Troczynski, T. Enhancing aluminum corrosion in water. *J. Appl. Electrochem.* **2009**, *39*, 1695. [CrossRef]
38. Razavi-Tousi, S.S.; Szpunar, J.A. Effect of addition of water-soluble salts on the hydrogen generation of aluminum in reaction with hot water. *J. Alloys Compd.* **2016**, *679*, 364–374. [CrossRef]
39. Zhu, L.; Zou, M.; Zhang, X.; Zhang, L.; Wang, X.; Song, T.; Wang, S.; Li, X. Enhanced Hydrogen Generation Performance of Al-Rich Alloys by a Melting-Mechanical Crushing-Ball Milling Method. *Materials* **2021**, *14*, 7889. [CrossRef] [PubMed]
40. Chen, C.; Guan, X.; Wang, H.; Dong, S.; Luo, P. Hydrogen generation from splitting water with Al–$Bi(OH)_3$ composite promoted by NaCl. *Int. J. Hydrogen Energy* **2020**, *45*, 13139–13148. [CrossRef]
41. Wang, H.-W.; Chung, H.-W.; Teng, H.-T.; Cao, G. Generation of hydrogen from aluminum and water—Effect of metal oxide nanocrystals and water quality. *Int. J. Hydrogen Energy* **2011**, *36*, 15136–15144. [CrossRef]
42. Dupiano, P.; Stamatis, D.; Dreizin, E.L. Hydrogen production by reacting water with mechanically milled composite aluminum-metal oxide powders. *Int. J. Hydrogen Energy* **2011**, *36*, 4781–4791. [CrossRef]
43. Deng, Z.-Y.; Tang, Y.-B.; Zhu, L.-L.; Sakka, Y.; Ye, J. Effect of different modification agents on hydrogen-generation by the reaction of Al with water. *Int. J. Hydrogen Energy* **2010**, *35*, 9561–9568. [CrossRef]
44. Razavi-Tousi, S.S.; Szpunar, J.A. Effect of structural evolution of aluminum powder during ball milling on hydrogen generation in aluminum–water reaction. *Int. J. Hydrogen Energy* **2013**, *38*, 795–806. [CrossRef]
45. Amrani, M.A.; Haddad, Y.; Obeidat, F.; Ghaleb, A.M.; Mejjaouli, S.; Rahoma, I.; Galil, M.S.A.; Shameeri, M.; Alsofi, A.A.; Saif, A. Productive and Sustainable H2 Production from Waste Aluminum Using Copper Oxides-Based Graphene Nanocatalysts: A Techno-Economic Analysis. *Sustainability* **2022**, *14*, 15256. [CrossRef]
46. Amrani, M.A.; Alrafai, H.A.; Al-nami, S.Y.; Obeidat, F.; Alwahbani, F.; Alhammadi, M.A.; Qasem, A. Green synthesis of Size-Controlled copper oxide nanoparticles as catalysts for H2 production from industrial waste aluminum. *Int. J. Energy Res.* **2022**, *46*, 14023–14035. [CrossRef]

47. Davies, J.; du Preez, S.P.; Bessarabov, D.G. On-Demand Hydrogen Generation by the Hydrolysis of Ball-Milled Aluminum–Bismuth–Zinc Composites. *Materials* **2022**, *15*, 1197.
48. Xiao, F.; Yang, R.; Li, J. Aluminum composites with bismuth nanoparticles and graphene oxide and their application to hydrogen generation in water. *Int. J. Hydrogen Energy* **2020**, *45*, 6082–6089. [CrossRef]
49. Jia, Y.; Shen, J.; Meng, H.; Dong, Y.; Chai, Y.; Wang, N. Hydrogen generation using a ball-milled Al/Ni/NaCl mixture. *J. Alloys Compd.* **2014**, *588*, 259–264. [CrossRef]
50. Davies, J.; Du Preez, S.P.; Bessarabov, D.G. The Hydrolysis of Ball-Milled Aluminum–Bismuth–Nickel Composites for On-Demand Hydrogen Generation. *Energies* **2022**, *15*, 2356.
51. du Preez, S.P.; Bessarabov, D.G. On-demand hydrogen generation by the hydrolysis of ball-milled aluminum composites: A process overview. *Int. J. Hydrogen Energy* **2021**, *46*, 35790–35813. [CrossRef]
52. Eom, K.S.; Kwon, J.Y.; Kim, M.J.; Kwon, H.S. Design of Al–Fe alloys for fast on-board hydrogen production from hydrolysis. *J. Mater. Chem.* **2011**, *21*, 13047–13051. [CrossRef]
53. Eom, K.; Kim, M.; Oh, S.; Cho, E.; Kwon, H. Design of ternary Al–Sn–Fe alloy for fast on-board hydrogen production, and its application to PEM fuel cell. *Int. J. Hydrogen Energy* **2011**, *36*, 11825–11831. [CrossRef]
54. Eom, K.; Cho, E.; Kwon, H. Feasibility of on-board hydrogen production from hydrolysis of Al–Fe alloy for PEMFCs. *Int. J. Hydrogen Energy* **2011**, *36*, 12338–12342. [CrossRef]
55. Kim, M.; Eom, K.; Kwon, J.; Cho, E.; Kwon, H. On-board hydrogen production by hydrolysis from designed Al–Cu alloys and the application of this technology to polymer electrolyte membrane fuel cells. *J. Power Sources* **2012**, *217*, 345–350. [CrossRef]
56. Kahveci, O.; Kaya, M.F. Hydrogen production from Al–Cu alloy using electric vehicle's waste DC motor coils. *Int. J. Hydrogen Energy* **2022**, *47*, 12179–12188. [CrossRef]
57. Wang, C.; Lin, K.; Liu, Y.; Chen, X.; Zou, H.; Qiu, C.; Yang, S.; Liu, X. Design and Fabrication of High Activity Retention Al-Based Composite Powders for Mild Hydrogen Generation. *Materials* **2019**, *12*, 3328. [CrossRef]
58. He, T.; Xiong, Y.; Du, S.; Yuan, Z.; Liang, X.; Huttula, M.; Cao, W. Impact of Li Addition in Al-Rich Alloys on Hydrogen Production in Water. *J. Mater. Eng. Perform.* **2019**, *28*, 2459–2464. [CrossRef]
59. Wang, S.; Zhu, L.; Zhang, L.; Zhang, X.; Wang, X.; Ge, M.; Li, X.; Zou, M. Preparation of Al-3Ga-3In-3Sn Alloy Powder by Coupling Alloying and Ball Milling and Its Application on High-Rate Hydrogen Generation at Room Temperature. *Metals* **2021**, *11*, 1704. [CrossRef]
60. Slocum, J.T.; Eagar, T.W.; Taylor, R.; Hart, D.P. Activation of bulk aluminum and its application in a hydrogen generator. *Appl. Energy* **2020**, *279*, 115712. [CrossRef]
61. Manilevich, F.D.; Pirskyy, Y.K.; Kutsyi, A.V.; Berezovets, V.V.; Yartys, V.A. Studies of Mechanochemically Activated Aluminum Powders for Generating Hydrogen from Water. *Powder Metall. Met. Ceram.* **2021**, *60*, 268–277. [CrossRef]
62. He, T.; Chen, W.; Wang, W.; Du, S.; Deng, S. Microstructure and hydrogen production of the rapidly solidified Al–Mg-Ga-In-Sn alloy. *J. Alloys. Compd.* **2020**, *827*, 154290. [CrossRef]
63. He, T.; Chen, W.; Wang, W.; Ren, F.; Stock, H.-R. Effect of different Cu contents on the microstructure and hydrogen production of Al–Cu-Ga-In-Sn alloys for dissolvable materials. *J. Alloys Compd.* **2020**, *821*, 153489. [CrossRef]
64. Du, B.D.; He, T.T.; Liu, G.L.; Chen, W.; Wang, Y.M.; Wang, W.; Chen, D.M. Al-water reactivity of AlMgGaInSn alloys used for hydraulic fracturing tools. *International Int. J. Hydrogen Energy* **2018**, *43*, 7201–7215. [CrossRef]
65. Barakat, M.A.; El-Sheikh, S.M.; Farghly, F.E. Regeneration of spent alkali from aluminum washing. *Sep. Purif. Technol.* **2005**, *46*, 214–218. [CrossRef]
66. Ambaryan, G.N.; Vlaskin, M.S.; Dudoladov, A.O.; Meshkov, E.A.; Zhuk, A.Z.; Shkolnikov, E.I. Hydrogen generation by oxidation of coarse aluminum in low content alkali aqueous solution under intensive mixing. *Int. J. Hydrogen Energy* **2016**, *41*, 17216–17224. [CrossRef]
67. Lim, S.T.; Sethupathi, S.; Alsultan, A.G.; Leong, L.K.; Taufiq-Yap, Y.H. Hydrogen Gas Production Using Aluminum Waste Cans Powder Produced by Disintegration Method. In *Key Engineering Materials*; Trans Tech Publications Ltd.: Bäch, Switzerland, 2020; pp. 228–234.
68. Porciúncula, C.; Marcilio, N.; Tessaro, I.; Gerchmann, M. Production of hydrogen in the reaction between aluminum and water in the presence of NaOH and KOH. *Braz. J. Chem. Eng.* **2012**, *29*, 337–348. [CrossRef]
69. Lluis Soler, J.; Munoz, M.; Casado, J. Aluminium and Aluminium alloy as sources of hydrogen for fuel cell application. *J. Power Sources* **2007**, *169*, 144–149. [CrossRef]
70. Alviani, V.N.; Hirano, N.; Watanabe, N.; Oba, M.; Uno, M.; Tsuchiya, N. Local initiative hydrogen production by utilization of aluminum waste materials and natural acidic hot-spring water. *Appl. Energy* **2021**, *293*, 116909. [CrossRef]
71. Martínez-Salazar, A.L.; Melo-Banda, J.A.; Coronel-García, M.A.; González-Barbosa, J.J.; Domínguez-Esquivel, J.M. Hydrogen generation by aluminum alloy corrosion in aqueous acid solutions promoted by nanometal: Kinetics study. *Renew. Energy* **2020**, *146*, 2517–2523. [CrossRef]
72. Alviani, V.N.; Setiani, P.; Uno, M.; Oba, M.; Hirano, N.; Watanabe, N.; Tsuchiya, N.; Saishu, H. Mechanisms and possible applications of the Al–H_2O reaction under extreme pH and low hydrothermal temperatures. *Int. J. Hydrogen Energy* **2019**, *44*, 29903–29921. [CrossRef]
73. Hiraki, T.; Takeuchi, M.; Hisa, M.; Akiyama, T. Hydrogen Production from Waste Aluminum at Different Temperatures, with LCA. *Mater. Trans.* **2005**, *46*, 1052–1057. [CrossRef]

74. Wang, X.; Zhang, Q.; Shi, X.; Wang, N.; Chai, Y. Synergistic effect of the fresh Co, Ni, and anion ions on aluminum or magnesium with water reactions. *Int. J. Energy Res.* **2019**, *43*, 430–438. [CrossRef]
75. Moreno-Flores, R.; Loyola-Morales, F.; Valenzuela, E.; Sebastian, P.J. Design and performance evaluation of a prototype hydrogen generator employing hydrolysis of aluminum waste. *Clean Technol. Environ. Policy* **2022**. [CrossRef]
76. Lim, S.T.; Sethupathi, S.; Alsultan, A.G.; Munusamy, Y. Hydrogen Production via Activated Waste Aluminum Cans and Its Potential for Methanation. *Energy Fuels* **2021**, *35*, 16212–16221. [CrossRef]
77. Chen, X.; Wang, C.; Liu, Y.; Zou, H.; Lin, K.; Yang, S.; Lu, Y.; Han, J.; Shi, Z.; Liu, X. Portable water-using H2 production materials converted from waste aluminum. *Energy Sources Part A Recovery Util. Environ. Eff.* **2018**, *40*, 1991–1997. [CrossRef]
78. Yolcular, S.; Karaoglu, S.; Karasoglu, M. Hydrogen generation performance of waste aluminum alloy chips and powders. *Energy Sources Part A Recovery Util. Environ. Eff.* **2022**, *44*, 1529–1540. [CrossRef]
79. Singh, K.; Meshram, A.; Gautam, D.; Jain, A. Hydrogen production using waste aluminium dross: From industrial waste to next-generation fuel. *Agron. Res.* **2019**, *17*, 1199–1206. [CrossRef]
80. Kale, M.; Yılmaz, İ.H.; Kaya, A.; Çetin, A.E.; Söylemez, M.S. Pilot-scale hydrogen generation from the hydrolysis of black aluminum dross without any catalyst. *J. Energy Inst.* **2022**, *100*, 99–108. [CrossRef]
81. Tang, W.; Yan, L.; Li, K.; Juan, Y.; Fu, C.; Zhang, J. A comparison study on aluminum-water reaction with different catalysts. *Mater. Today Commun.* **2022**, *31*, 103517. [CrossRef]
82. Szklarska-Smialowska, Z. Pitting corrosion of aluminum. *Corros. Sci.* **1999**, *41*, 1743–1767. [CrossRef]
83. Vijh, A.K. The corrosion potentials of some common metals in oxygenated solutions in relation to semi-conductivity of the corrosion films*. *Corros. Sci.* **1972**, *12*, 105–111. [CrossRef]
84. Wu, S.; Cai, X.; Cheng, Y.; Zhou, L. Evolution of Intermetallic Cu_9Al_4 During the Mechanical Alloying of Cu-Al Mixtures in High-Energy Ball Milling. *J. Electron. Mater.* **2021**, *50*, 4549–4556. [CrossRef]
85. Xi, S.; Zhou, J.; Zhang, D.; Wang, X. Solid-state synthesis reaction between Al and Cu powders during ball milling. *Mater. Lett.* **1996**, *26*, 245–248. [CrossRef]
86. Zhang, D.L.; Ying, D.Y. Solid state reactions in nanometer scaled diffusion couples prepared using high energy ball milling. *Mater. Sci. Eng. A* **2001**, *301*, 90–96. [CrossRef]
87. Sviridova, T.A.; Shevchukov, A.P.; Shelekhov, E.V.; Borisova, P.A. Use of mechanical alloying and subsequent annealing for obtaining intermetallic compound CuAl2. *Phys. Met. Metallogr.* **2011**, *112*, 356. [CrossRef]
88. Makhlouf, M.B.; Bachaga, T.; Sunol, J.J.; Dammak, M.; Khitouni, M. Synthesis and Characterization of Nanocrystalline Al-20 at. % Cu Powders Produced by Mechanical Alloying. *Metals* **2016**, *6*, 145. [CrossRef]
89. Besson, R.; Avettand-Fènoël, M.N.; Thuinet, L.; Kwon, J.; Addad, A.; Roussel, P.; Legris, A. Mechanisms of formation of Al4Cu9 during mechanical alloying: An experimental study. *Acta Mater.* **2015**, *87*, 216–224. [CrossRef]
90. Grigoreva, T.F.; Petrova, S.A.; Kovaleva, S.A.; Kiseleva, T.Y.; Zholudev, S.I.; Vosmerikov, S.V.; Udalova, T.A.; Devyatkina, E.T.; Polyakov, S.N.; Lyakhov, N.Z. Mechanochemical Formation of Solid Solution of Aluminum in Copper. *Phys. Met. Metallogr.* **2021**, *122*, 370–375. [CrossRef]
91. de la Rosa, F.; Romero-Romero, J.R.; López-Miranda, J.L.; Hernández-Torres, A.G.; Rosas, G. Phase transformation of the $CuAl_2$ intermetallic alloy during high-energy ball-milling. *Intermetallics* **2015**, *61*, 51–55. [CrossRef]
92. Matvienko, Y.; Rud, A.; Polishchuk, S.; Zagorodniy, Y.; Rud, N.; Trachevski, V. Effect of graphite additives on solid-state reactions in eutectic Al–Cu powder mixtures during high-energy ball milling. *Appl. Nanosci.* **2020**, *10*, 2803–2811. [CrossRef]
93. Vieira, A.C.; Pinto, A.M.; Rocha, L.A.; Mischler, S. Effect of Al2Cu precipitates size and mass transport on the polarisation behaviour of age-hardened Al–Si–Cu–Mg alloys in 0.05M NaCl. *Electrochim. Acta* **2011**, *56*, 3821–3828. [CrossRef]
94. Razavi-Tousi, S.S.; Szpunar, J.A. Mechanism of Corrosion of Activated Aluminum Particles by Hot Water. *Electrochim. Acta* **2014**, *127*, 95–105. [CrossRef]
95. Razavi-Tousi, S.S.; Szpunar, J.A. Role of Ball Milling of Aluminum Powders in Promotion of Aluminum-Water Reaction to Generate Hydrogen. *Metall. Mater. Trans. E* **2014**, *1*, 247–256. [CrossRef]
96. Razavi-Tousi, S.S.; Szpunar, J.A. Effect of ball size on steady state of aluminum powder and efficiency of impacts during milling. *Powder Technol.* **2015**, *284*, 149–158. [CrossRef]
97. Grosjean, M.H.; Zidoune, M.; Roué, L.; Huot, J.Y. Hydrogen production via hydrolysis reaction from ball-milled Mg-based materials. *Int. J. Hydrogen Energy* **2006**, *31*, 109–119. [CrossRef]
98. Xiao, F.; Yang, R.; Gao, W.; Hu, J.; Li, J. Effect of carbon materials and bismuth particle size on hydrogen generation using aluminum-based composites. *J. Alloys Compd.* **2020**, *817*, 152800. [CrossRef]
99. Sha, G.; Marceau, R.K.W.; Gao, X.; Muddle, B.C.; Ringer, S.P. Nanostructure of aluminium alloy 2024: Segregation, clustering and precipitation processes. *Acta Mater.* **2011**, *59*, 1659–1670. [CrossRef]
100. Staszczyk, A.; Sawicki, J.; Adamczyk-Cieslak, B. A Study of Second-Phase Precipitates and Dispersoid Particles in 2024 Aluminum Alloy after Different Aging Treatments. *Materials* **2019**, *12*, 4168. [CrossRef]
101. Brown, M.E. (Ed.) *Handbook of Thermal Analysis and Calorimetry*; Elsevier Science B.V.: Amsterdam, The Netherlands, 1998; Volume 1.
102. Hay, M.B.; Myneni, S.C.B. Geometric and Electronic Structure of the Aqueous $Al(H_2O)_6^{3+}$ Complex. *J. Phys. Chem. A* **2008**, *112*, 10595–10603. [CrossRef]

103. Qi, T.; He, M.-F.; Zhu, L.-F.; Lyu, Y.-J.; Yang, H.-Q.; Hu, C.-W. Cooperative Catalytic Performance of Lewis and Brønsted Acids from $AlCl_3$ Salt in Aqueous Solution toward Glucose-to-Fructose Isomerization. *J. Phys. Chem. C* **2019**, *123*, 4879–4891. [CrossRef]
104. Wan, S.; Song, X.; Wang, X.; Yuan, C.; Wang, B.; Chen, H.; Li, Y.; Ouyang, K.; Chen, R. Enhanced removal thallium from rinsing wastewater by poly aluminum chloride: Experimental and theoretical studies. *Sep. Purif. Technol.* **2022**, *302*, 122158. [CrossRef]
105. Zhang, W.-M.; Zhuang, J.-X.; Chen, Q.; Wang, S.; Song, W.-G.; Wan, L.-J. Cost-Effective Production of Pure Al13 from $AlCl_3$ by Electrolysis. *Ind. Eng. Chem. Res.* **2012**, *51*, 11201–11206. [CrossRef]
106. Morris, C.E.; Welch, C.M. Use of Aluminum or Titanium Compounds to Bind Antibacterial Agents to Cotton Fabric. *Text. Res. J.* **1983**, *53*, 143–147. [CrossRef]
107. Ivanov, V.V.; Kirik, S.D.; Shubin, A.A.; Blokhina, I.A.; Denisov, V.M.; Irtugo, L.A. Thermolysis of acidic aluminum chloride solution and its products. *Ceram. Int.* **2013**, *39*, 3843–3848. [CrossRef]

Disclaimer/Publisher's Note: The statements, opinions and data contained in all publications are solely those of the individual author(s) and contributor(s) and not of MDPI and/or the editor(s). MDPI and/or the editor(s) disclaim responsibility for any injury to people or property resulting from any ideas, methods, instructions or products referred to in the content.